MEG liquid xenon detector

S Mihara

KEK IPNS, 1-1 Oho, Tsukuba, Ibaraki 305-0801, Japan

E-mail: satoshi.mihara@kek.jp

Abstract. We constructed a gamma-ray detector using 900 L of liquid xenon to identify a 52.8-MeV gamma ray from the lepton-flavor violating muon decay, $\mu \rightarrow e\gamma$. The detector uses only scintillation light originating from liquid xenon to reconstruct the gamma-ray energy, interaction position, and arrival time. A new photomultiplier that can be operated in liquid xenon has been newly developed for this detector. Details of the detector is described in this paper along with the present performance of the detector.

1. Introduction

Liquid xenon is believed to be an excellent material for gamma-ray detection because of its suitable features such as high density, efficiency and decay time of scintillation light emission and high transparency for the light. To achieve large acceptance with good uniformity, it is beneficial for the liquid to be stably maintained at pressures around the atmospheric pressure in a cryostat equipped with a refrigerator with moderate cooling power. The ionization charge induced in liquid xenon is also commonly used for gamma-ray and/or charged particle measurement, although the detector response becomes slow for such measurements because of the limited electron drift speed in the liquid. A hybrid method that combines scintillation light and ionization charge measurements has been studied to improve the performance of a detector. Extensive studies have beeen conducted to enable the use of such new detectors in many applications [1, 2].

2. MEG experiment

The mu-e-gamma (MEG) experiment aims at detecting a lepton-flavor violating $\mu^+ \rightarrow e^+\gamma$ decay with higher sensitivity than that obtained in the previous experiment, in which the limit was set at 1.2×10^{-11} at 90% confidence level (CL)[3]. The ultimate aim of the MEG experiment is to achieve a sensitivity of 10^{-13} for the Br($\mu^+ \rightarrow e^+\gamma$) [4].

The signal of $\mu^+ \rightarrow e^+\gamma$ is a simultaneous emission of a positron and a gamma ray, each with an energy equivalent to half of the muon mass, 52.8 MeV, at an opening angle of 180°. The gamma ray is detected by a liquid xenon photon detector, which is described in detail in this paper. A positron detector is composed of a drift chamber tracking system [5], time measuring counter system [6], and super-conducting magnet with a gradient magnetic field [7].

There are two major background sources in this experiment. One is the radiative muon decay, $\mu^+ \rightarrow e^+\nu_e\bar{\nu_\mu}\gamma$, in which two neutrinos carry tiny amounts of energy. The other is an accidental overlap of an electron emission from the Michel decay, $\mu^+ \rightarrow e^+\nu_e\bar{\nu_\mu}$, and a gamma-ray emission from a radiative muon decay or positron annihilation in flight.

The setup of the experiment is shown in Figure 1. Muon beam is provided at the PiE5 beam line of Paul Scherrer Institute (PSI), where the world's most intense surface muon beam is available. The PSI proton accelerator generates a 580-MeV 2-mA proton beam that creates pions and muons as daughter particles of the pions. The repetition cycle of the proton is 19.75 ns, which is smeared by the pion life time (26 ns), resulting in the generation of a quasi-continuous muon beam that is used in the experiment. The muon beam is transported to the experimental area and filtered by an electrostatic Wien filter to remove positron contamination. The beam is focused and stopped on a muon stopping target located at the center of the spectrometer magnet.

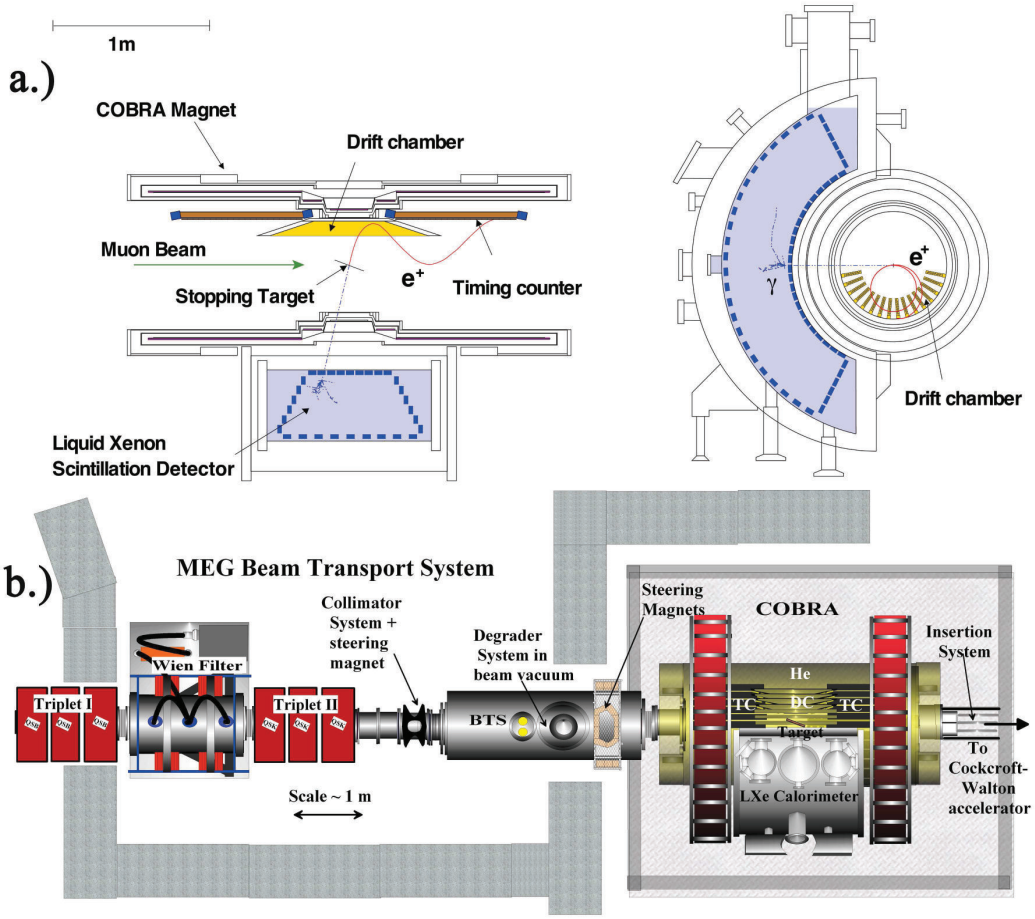

Figure 1. Schematic of MEG experiment. a) Details of positron spectrometer and photon detector. b) MEG beam transport system.

The target is surrounded by a positron tracking system composed of 16 drift chamber modules; this system measures the positron momentum and predicts the hit position on the timing counters located at both ends of the magnet. The liquid xenon detector is located at the right of the beam line beside the spectrometer magnet and measures the gamma ray originating from the target. The detector covers 10% of the acceptance with good uniformity.

The construction of the experimental setup was completed in 2007 followed by a short engineering run. In 2008 and 2009, physics data were acquired using the completed setup.

The result obtained using the 2008 data has been recently published; in this result the limit on Br($\mu^+ \rightarrow e^+\gamma$) was set at 2.8×10^{-11} (90% CL)[8]. Currently, the analysis of 2009 data is in progress, and further acquisition of physics data is continuing in 2010 and is expected to continue in future years.

3. MEG liquid xenon photon detector

A schematic view of the MEG xenon photon detector is shown in Figure 2. The detector measures gamma rays from the muon stopping target by using liquid xenon as the scintillation material. We do not use ionization charge information but use only scintillation light for the measurement. Consequently, the detector can be quite simple, and the detector can provide a reasonably fast response, which is essential for searching a rare decay mode. A total of 900 L of liquid xenon is used in the detector. The active volume is viewed from all sides by photomultipliers operational in the liquid. The gamma-ray energy is evaluated by summing the charge integration of all photomultiplier signals, position of gamma-ray first interaction positions in the liquid is evaluated by weighting the photomultiplier positions on the inner (gamma-ray entrance) side with the observed charge, and gamma-ray arrival time is estimated by using the time information of the photomultiplier signals. Waveforms of all photomultipliers are recorded using waveform digitizers that are newly developed for the experiment [9]. Details of the detector components are described in this section.

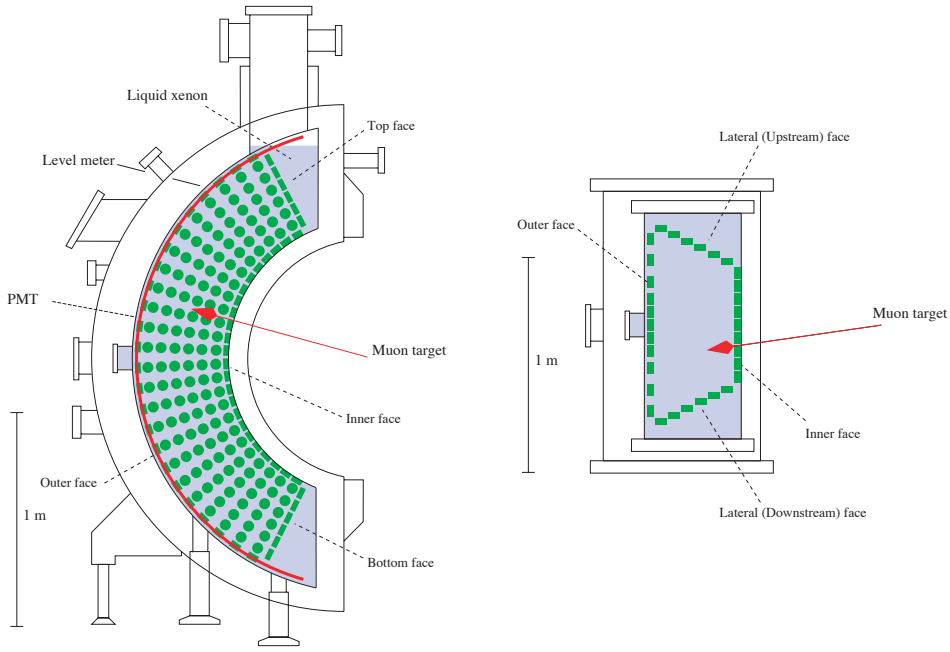

Figure 2. Schematic views of MEG liquid xenon photon detector. Side (left) and top (right) views.

3.1. Prototype R&D

The detector has been constructed after carrying out numerous R&D activities using two prototypes with different sizes. The first prototype was constructed to demonstrate the principle of the detector, that is, the measurement of gamma rays using only liquid xenon scintillation light by photomultipliers submersed in the liquid. This prototype has an active volume of 2.3 L viewed by 32 photomultipliers. The detector response was investigated by using gamma

rays below 2 MeV from radioactive sources, and this response was compared with a simulation incorporating energy loss of gamma rays in liquid xenon and the scintillation light emission and transmission in the liquid [10].

The second prototype was constructed to demonstrate the detector performance for higher energy gamma rays around 50 MeV and to gain the operation experience required to conduct the $\mu^+ \rightarrow e^+\gamma$ search experiment, which runs for several months once the physics data acquisition is started. The second prototype has an active volume of 68.6 L surrounded by 228 photomultipliers. The detector performance was investigated by using gamma beams up to 40 MeV generated in inverse-Compton scatterings and also using electron beams up to 60 MeV [11]. A sophisticated technique to calibrate photomultipliers in liquid xenon has been developed in this prototype [15] together with a purification method to remove impurities such as water, oxygen, and nitrogen that can affect scintillation light emission and transmission [16, 17]. A method to evaluate the light absorption, separately from elastic scattering of light, has also been developed [13].

3.2. Detector construction

The MEG liquid xenon photon detector consists of the following components:

(i) Photomultiplier to detect scintillation light of liquid xenon
(ii) Cryostat and refrigerator to maintain liquid xenon in a stable state
(iii) Xenon purifier to remove impurities possibly contained in xenon
(iv) Xenon storage to store xenon during detector maintenance

The photomultiplier (Hamamatsu R9869) has been developed for use in the MEG liquid xenon photon detector. This photomultiplier uses a metal-channel dynode structure to achieve a reasonable electron multiplication gain ($>10^6$) inside a short package (height: 3.2 cm) and a high tolerance against the magnetic field as large as 100 G, as shown in Figure 3. The package is made of stainless steel, which allows the photomultiplier body to be pressure resistant up to 0.3 MPa. The photocathode was carefully designed to minimize the reduction in the quantum efficiency in the liquid xenon temperature range (165–167 K). Electronic parts used in the bleeder circuit have been carefully selected to minimize the influence of outgassing impurities from these parts. The diagram of the bleeder circuit is shown in Figure 4. Heat dissipation from the bleeder circuit is minimized by optimizing the resister chain (16 MΩ) with zener diode protection in the last two dynodes, which keeps the voltage constant under a high counting rate environment. In the MEG liquid xenon detector, 846 photomultipliers are used. They are first installed to separate holders and then assembled in the detector cryostat. There are five differnt types of holders: top, bottom, lateral, outer, and inner. The top and bottom face holders are identical, and they hold 54 photomultipliers each. The lateral face holders have a trapezoidal shape and hold 6 photomultipliers each. The outer face hodlers have a simple rectangular shape and hold 9 photomultipliers each, except at the central part where the photomultiplier density is maintained higher than that at the other parts for calibration purposes. The inner face holders are fabricated in such a manner that the amount of material used is reduced and the liquid xenon penetration is minimized to avoild gamma-ray interaction inside the holder. The holder body is made of PEEK and the other parts are primarily made of plastic. The photomultiplier cables are molded in expoxy glue, and the remaining space around the bleeder circuit of the photomultipliers is filled with glass beads. Each inner face holder contains 9 photomultipliers, and a minimum possible distance is maintained between neighboring photomultipliers.

For photomultiplier calibration, blue LEDs with different light attenuations are installed on the photomultiplier holders so that the photomultipliers can be illuminated uniformly with different light intensities. Five gold-plated tungsten wires of 100-μm diameter are permanently suspended in the active volume and fixed on the photomultiplier holders; five ^{241}Am alpha souces

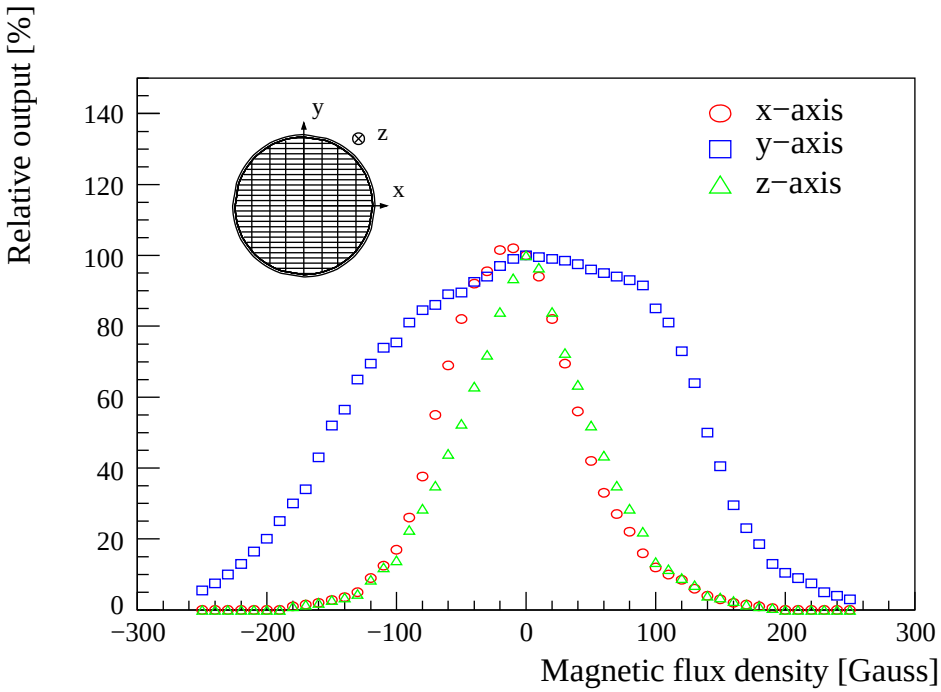

Figure 3. Tolerance of photomultiplier (Hamamatsu R9869) used in MEG liquid xenon detector against magnetic field.

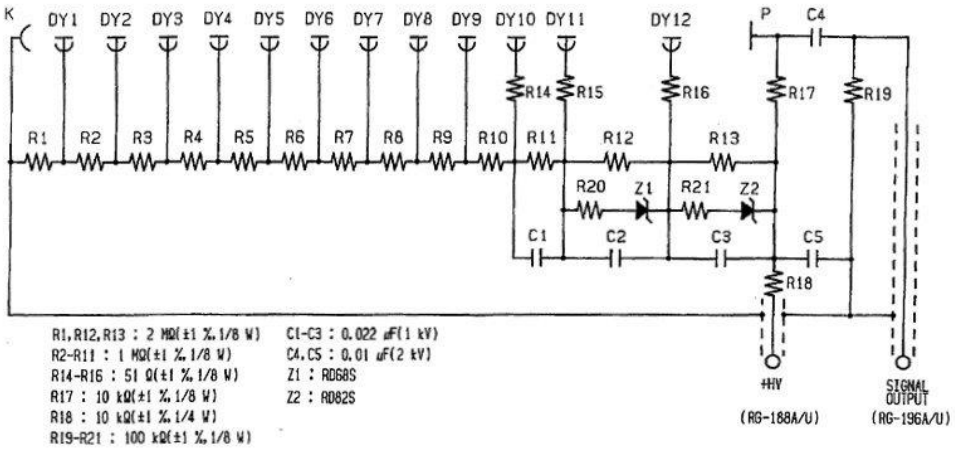

Figure 4. Bleeder circuit diagram of photomultiplier (Hamamatsu R9869).

are deposited on each of these wires [15]. Figure 5 (left) shows a micropicture of the souce, and Figure 5 (right) shows a photograph of a suspended wire in the second prototype. In the MEG liquid xenon detector, wires are suspended in a similar manner. Alpha particles with fixed energy are constantly emitted from the sources and thereby a constant amount of scintilaltion light is emitted regularly. Because of the difference in the mechanisms of scintillation light emission, the photomultiplier waveforms for the gamma-ray and alpha events are different, and thus, the alpha source signal can be easily separated from the gamma-ray signals.

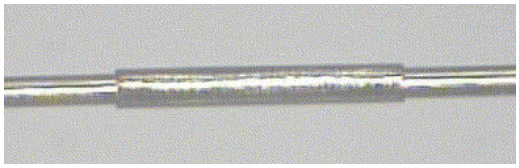

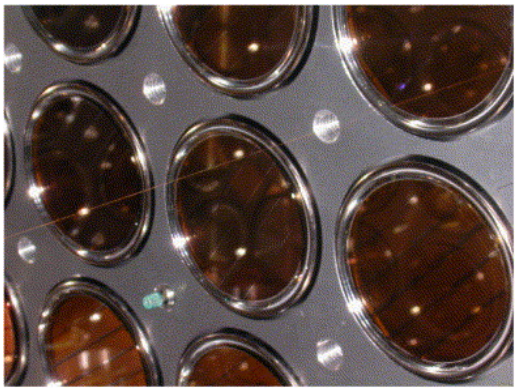

Figure 5. ^{241}Am alpha source deposited on 100-μm gold-plated tungsten wire (left) and source wire fixed on photomultiplier holder in second prototype (right).

The detector is C-shaped; this shape enables the detector to cover the acceptance uniformly. Therefore, the cryostat, which contains liquid xenon is also C-shaped, as shown in Figure 2. The cryostat is composed of an inner vessel that contains liquid xenon and an outer vessel for vacuum heat insulation. The wall thickness of the gamma-ray entrance side in the outer vessel is kept small (400 μm, stainless steel) to reduce gamma-ray interaction with the wall. The thickness of the wall of the inner vessel is also restricted to 400 μm and is made of the same stainless steel material; this wall is backed by a honeycomb panel sandwiched between two carbon fiber sheets. The panel was specially developed for the MEG liquid xenon detector. The honeycomb itself is made of aluminum with a cell thickness of 0.0254 mm, size of 4.67 mm, and height of 19 mm. Each carbon fiber sheet is composed of 8 layers of prepreg and has a thickness of 0.13 mm. These layers are glued together to form a sheet using two-component epoxy adhesive, which is known to be used at low temperatures. The specifications of the panel is summarized in Table 1. The panel is fixed to the inner vessel with screws at the edges of the panel, as shown in Figure 6 (left). The most difficult part of the panel design is to devise a method to transit the thickness of the panel from the inner area where the aluminum honeycomb exists (thick part) to the edges of the panel where only carbon fiber sheets are stacked (thin part), as illustrated in Figure 7. The total force that is applied perpendicular to the panel by the xenon pressure

Figure 6. Honeycomb panel fixed on inner vessel (left) and reinforcement parts installed at panel edge (right).

is as large as 80 kN. This would cause a huge shearing force at the transition area, which is almost at the limit of the carbon fiber strength. Therefore, we added some reinforcement parts, as shown in Figure 6 (right), to the transition area to induce a change in the direction of the force applied at the edge. The honeycomb backing enables us to operate the detector up to pressure of 0.2 MPa when the thermal insulation layer evacuated. The cryostat is equipped with a rapture disk to blow the xenon gas when the pressure reaches 0.19 MPa. The outlet of the rupture disk is connected to a check valve to save the xenon gas when the pressure decreases below 0.16 MPa.

Table 1. Specifications of honeycomb panel used in MEG liquid xenon detector.

Honeycomb material	Aluminum 5052
Hexagonal cell thickness	0.0254 mm
Hexagonal cell size	4.76 mm
Hexagonal cell height	19 mm
Carbon fiber sheet	T300 (Toray)
Carbon fiber sheet thickness	1.5 mm
Prepreg layers per sheet	0.13 mm $\times$ 8
Glue	EA 9361 (Hysol)

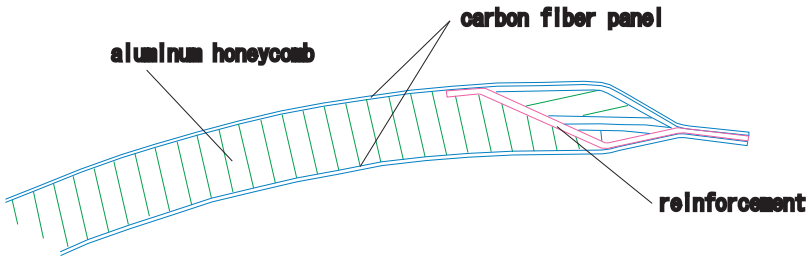

Figure 7. Cross section of transition area of carbon-fiber honeycomb panel.

A pulse-tube refrigerator is mounted on the cryostat to enable the recondensation of xenon. The refrigerator has been developed by our group [1] and is optimized for cooling liquid xenon to around 165 K. It has a cooling power of 200 W at 165 K without any electrical noise nor mechanical vibration thanks to the cooling principle of the pulse-tube refrigerator [12]. The refrigerator itself does not require maintenance, enabling us to preserve the purity of liquid xenon once it is purified. Liquid nitrogen cooling pipes are used to enable the refrigerator to achieve efficent cooling. One spiral pipe is installed around the refrigerator mounted on a central chimney, another pipe is welded on to the outer surface of the wall of the inner vessel, and one pipe each is welded on to the outer surfaces of the upstream and downstream covers of the inner vessel. The pipes on the outer surfaces of the wall and covers (Figure 8) are used particularly for pre-cooling the vessel before it is filled with liquid xenon.

[1] Currently, the refrigerator of this type is produced by Iwatani Co. Ltd.

Figure 8. Cooling pipes welded on the outer surfaces of the wall (left) and covers (right).

Impurity removal from liquid xenon is an important issue that should be addressed to achieve the best performance of the detector [13]. Scintillation light is known to be emitted in liquid xenon according to the following mechanism [18]:

$$\mathrm{Xe}^* + \mathrm{Xe} \rightarrow \mathrm{Xe}_2^* \rightarrow 2\mathrm{Xe} + h\nu$$

or

$$\mathrm{Xe}^+ + \mathrm{Xe} \rightarrow \mathrm{Xe}_2^+$$

$$\mathrm{Xe}_2^+ + \mathrm{e} \rightarrow \mathrm{Xe} + \mathrm{Xe}^{**}$$

$$\mathrm{Xe}^{**} \rightarrow \mathrm{Xe}^* + \mathrm{heat}$$

$$\mathrm{Xe}^* + \mathrm{Xe} \rightarrow \mathrm{Xe}_2^* \rightarrow 2\mathrm{Xe} + h\nu$$

Because a bound Xe_2 ground state does not exit, xenon molecules themselves do not absorb light. However, electronegative impurities such as oxygen and nitrogen, if present in the liquid, can affect light emission by disturbing the recombination process. Oxygen contamination can also affect the transmission of the scintillation light because the light absorption cross section of oxygen overlaps the spectrum of the scintillation light originating from xenon. Water contamination affects scintillation light transmission to a larger extent than oxygen because of the significant overlap of the absorption cross section of water with the spectrum [13]. In order to remove these impurity molecules, three types of vacuum pumps and gas and liquid purifiers are included in the experimental system.

Evacuation of the cryostat is carried out before pre-cooling, first by using a turbo-molecular pump with a pumping speed of 400 L/h down to a presssure of 10^{-2} Pa, and then by operating a cryopump with a pumping speed of 2500 L/s for water removal along with the turbo-molecular pump operation. Because the cryostat contains photomultipliers that cannot be heated above 50 °C, use of the cryopump is very beneficial for removing water molecules from the cryostat. After the vacuum level reaches 10^{-3} Pa, a getter pump starts operation to achieve vacuum levels below 10^{-4} Pa.

Liquid xenon is filled in the inner vessel after evacuation and pre-cooling. Although the vessel is evacuated sufficiently good from the view point of remaining gas ratio to the amount of used xenon, impurity molecules that have been captured on the surface of material in the cryostat

dissolve into the liquid after liquid filling. These impurities are removed by using the xenon purification system. The purification system has two purifiers, as mentioned previously. One is a metal-heated getter purifier that can remove almost all types of gas molecules except rare gase molecules. Xenon extracted from the cryostat is evaporated, transferred to the purifier, and then returned to the cryostat to be liquefied again. A diaphragm pump is used to circulate xenon without introducing any additional impurities. In this purification method, the speed of gas circulation is limited by the cooling power, resulting in a purification speed of 0.06 L/h, which is not sufficient to purify 900 L of liquid xenon. The other purifier is a copper-based purifier that is used to remove impurities in the liquid phase. A faster purification speed can be achieved by using this purifiers because of the lower amount of heat inflow during xenon circulation. Liquid xenon is transferred to a purifier cryostat located beside the detector through a drain at the bottom of the detector; the purified xenon is returned to the detector cryostat through two purifier cartridges. One of the cartridges is the main purifier filled with pure copper that removes impurities by oxidization. The other cartridge is filled with molecular sieves with a pore size of 13A to enable the removal of water molecules. A centrifugal pump that is designed for use with liquid xenon is employed to circulate the liquid; this enables us to achieve a purification speed of 70 L/h.

The components required for detector operation have already been described above, but there is another component that is required when the experiment is being performed. This is the xenon storage system that is used to store xenon during detector maintenance [14]. Xenon is stable at 5.8 MPa with a density of 1.1 g/cm^3 at 17 ^{o}C (critical point). In the MEG experiment, eight high-pressure tanks are used to store xenon, each of which can contain up to 360 kg of xenon corresponding to 120 L of liquid xenon. Recovery of xenon is carried out in the tanks by cooling the tanks with liquid nitrogen, which freezes xenon in the tanks. The vapor pressure of solid xenon is almost zero; thus, we can recover xenon from the detector with minimum loss. This high-pressure tank storage system is simple and safe, but it takes more than one week to transfer xenon from the detector to the tanks. Such a long transfer period is not acceptable in case of an emergency such as the breakdown of the insulation vacuum during operation. To solve this problem, a cryogenic tank with a volume of 1100 L is connected to the system so that xenon can be transferred from the detector using the centrifugal pump of the purification system. The cyogenic tank is equipped with a pulse-tube refrigerator as well as a liquid nitrogen cooling pipe for pressure control. The incoming heat while maintaining xenon at 165 K is estimated to be less than 20 W, which is sufficiently small to be cooled by using only the refrigerator. In addition, the cryogenic tank is designed such that it can tolerate pressure of up to 0.6 MPa; thus, xenon can be stored safely without the supply of cooling power for 100 h. Figure 9 shows a schematic view of the purification and storage system. In this system, xenon can be recovered to the cryogenic tank within two days. Xenon is transferred from the cryogenic tank to the detector by maintaining a pressure difference between them. The xenon pressure in the cryogenic tank can be increased using a heater equipped at the bottom of the tank.

3.3. Detector operation

Before starting detector operation, the detector cryostat is evacuated sufficiently, as previously described. Simultanneously, xenon is liquefied in the cryogenic tank using the pulse-tube refrigerator and by liquid nitrogen cooling. Liquid xenon is subsequently transferred from the cryogenic tank to the detector, and the operation is started. After the detector cryostat is filled with liquid xenon, the gas pressure is controlled using a heater and by liquid nitrogen cooling with continuous operation of the pulse-tube refrigerator. The heater reduces the refrigerator cooling power whereas liquid nitrogen cooling is used to increase the cooling power. The detector status is continuously monitored and controlled by a system developed for the MEG experiment. This control system uses one microcontroller in a single node that can handle multichannel inputs

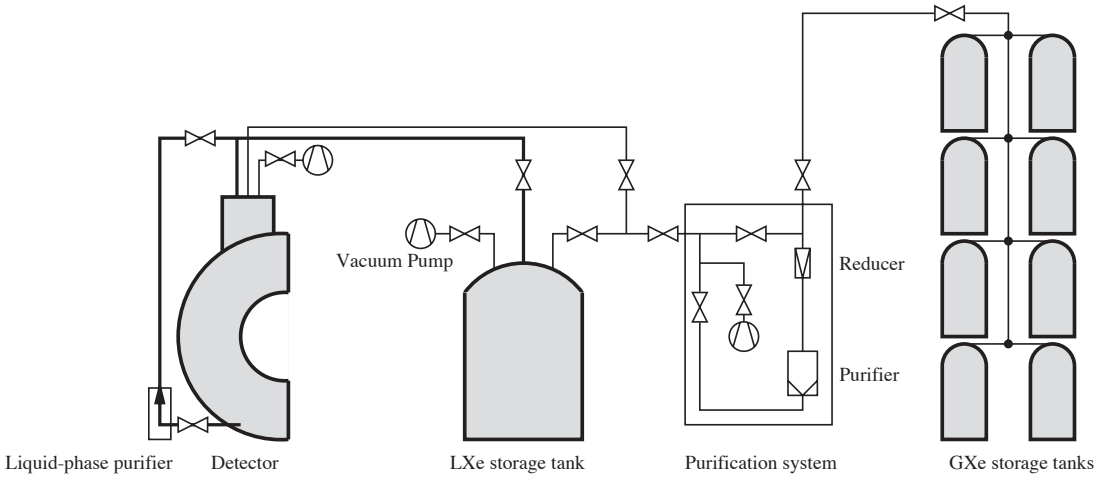

Figure 9. Xenon purification and storage system.

and outputs. All nodes are connected to the Ethernet and are integrated to the data acquisition system. The system periodically records the detector status on data files so that the online detector status can be inspected easily while performing data analysis.

The calibration of the detector is carried out in several steps. Among these steps, photomultiplier calibration is the most basic and important step. The behavior of the photomultipliers has to be carefully measured and calibrated under realistic operating conditions. The gain of the photomultipliers is determined by flashing blue LEDs in liquid xenon. The quantum efficiencies of the photomultipliers are determined using scintillation light induced by alpha sources installed in the active volume [15]. The measurement result of the alpha source signal is compared with a simulation result that incorporates information regarding energy loss, scintillation light emission, and scintillation light transmission in the liquid [15]. The determination of the quantum efficiencies is carried out using an iteration process because there are at least two undefined parameters in the system, i.e., the absorption length of the scintillation light in the liquid and the quantum efficiencies. These parametes are determined step by step and more precise results are obtained as the iteration process continues. In this process, photomultiplier calibration data in cold gas xenon is used to determine the initial parameter of quantum efficiencies because scintillation light transmission in gas is not affected by the Rayleigh scattering which in liquid has to be carefully treated. Furthermore, an Am-Be radioactive source has recently been used for more precise determination of the quantum efficiencies of the photomultipliers.

The detector response to higher energy gamma rays is investigated using gamma rays of 17.6 MeV obtained from a reaction of p(Li, Be)γ, which is resonant at E_p = 440 keV with a width of approximately 15 keV, and also from π^0 decays produced via a charge exchange process $\pi^- + p \rightarrow \pi^0 + n$. For using the gamma rays obtained from the p(Li, Be)γ reaction, a Cockcroft-Walton (CW) proton accelerator is installed at the rear end of the experimental area. The accelerator can provide 1–100-μA 300–900-keV protons to a LiF target that can be positioned at the center of the detector by a linear motion system. The specifications of the CW accelerator are summarized in Table 2. Fig. 10 shows the detector response to 17.6-MeV gamma rays. This calibration is repeated three times a week to monitor the change of the detector status and offline corrections.

The detector performance to the signal gamma ray (52.8 MeV) is evaluated by using 54.9-MeV

Table 2. Specifications of MEG CW accelerator.

	Nominal	Measured at PSI
Terminal energy range	300–900 keV	200–1100 keV
Energy ripple	<500 V_{rms}	<50 V_{rms}
Angular divergence	<(5×5) $mrad^2$	∼(4×4) $mrad^2$
Spot size at 3 m	<(3×3) cm^2	<(1×1) cm^2
Energy setting reproducibility	0.1%	OK
Energy stability FWHM	0.1%	OK
Range of current	1–100 μA	0.1–135 μA
Current stability	3%	OK
Current reproducibility	10%	OK
Start-up time	<20 m	<15 m

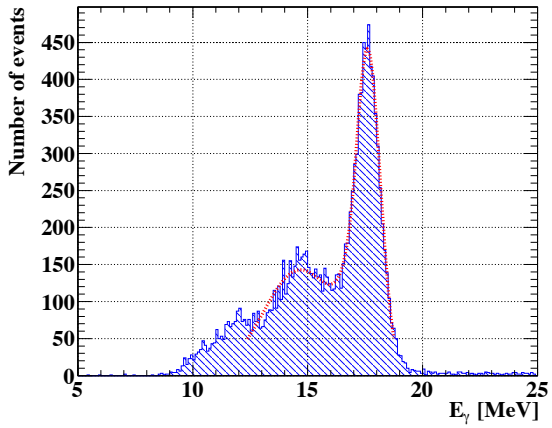

Figure 10. Detector response to 17.6-MeV gamma rays obtained from p(Li, Be)γ

gamma rays originating from the π^0 decays and by carrying out an extrapolation based on the Monte Carlo simulation from 54.9 to 52.8 MeV. The production of π^0 is realized through a charge exchange (CEX) process $\pi^- + p \rightarrow \pi^0 + n$. For executing this calibration, the beam line setting is modified to provide a π^- beam. A liquid hydrogen target with a pressure control using liquid helium replaces the muon stopping target. For identifying the 54.9-MeV gamma rays originating from π^0 decays, an NaI counter composed of 9 crystals, each of which has a dimension of 62.5 × 62.5 × 305 mm^3, and equipped with an avalanche photodiode readout is installed on the opposite side of the magnet to the liquid xenon detector. The counter is mounted on a three-dimensionally movable stage to detect $\pi^0 \rightarrow \gamma\gamma$ decays with the opening angle between two gamma rays close to 180° over the acceptance of the liquid xenon detector. Two plastic scintillation counters with lead converters are placed in front of the NaI counter for carrying out time calibration. The setup of the CEX calibration is schematically shown in Figure 11.

Figure 12 shows a distribution of π^0 data measured using the liquid xenon detector and the NaI counter. The opening angle between two gamma rays originating from π^0 decays is selected to be approximately 180°, thus providing gamma ray energy close to both edges of energy

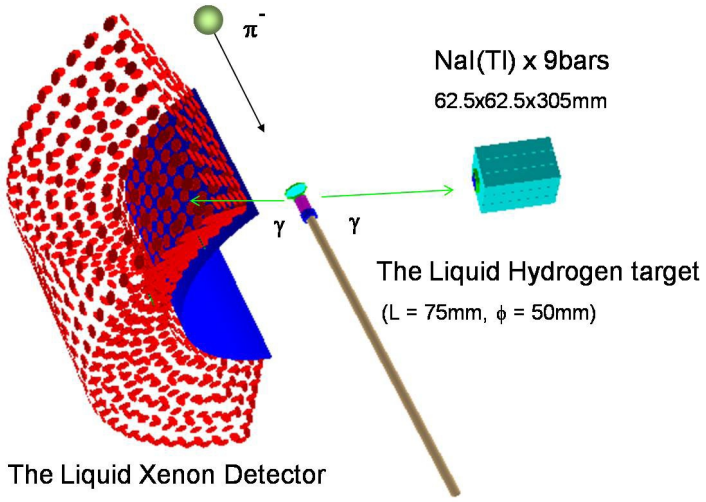

Figure 11. Experimental setup for CEX calibration.

distribution ranging from 54.9 to 82.9 MeV. By requiring 82.9 MeV gamma-ray detection on the NaI counter, semi-monochromatic gamma-rays of 54.9 MeV can be prepared on the liquid xenon detector side.

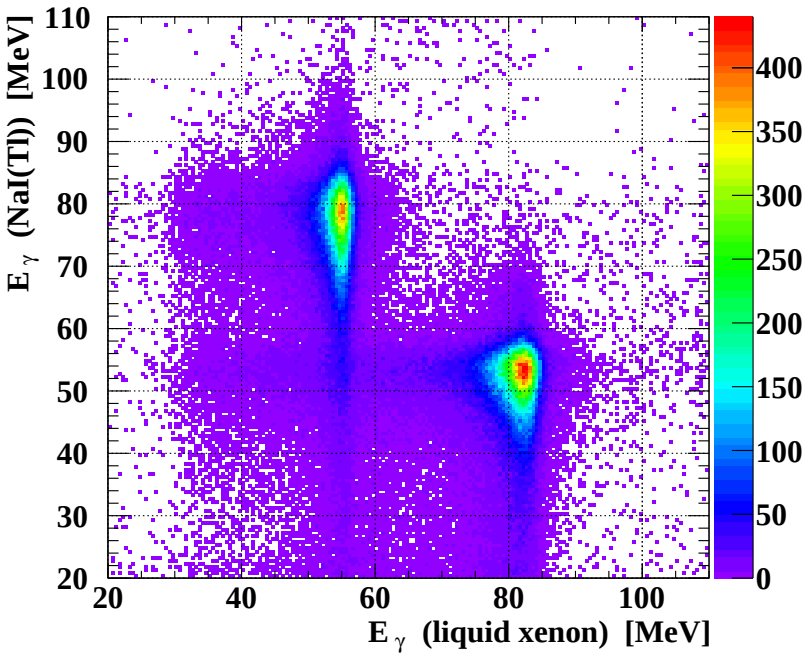

Figure 12. Gamma-ray energy distributions from CEX π^0 decays observed in the liquid xenon photon detector and NaI counter.

MEG data is taken with a trigger requirement both on the liquid xenon detector and positron detector. It is also required that the gamma ray and the positron be emitted back to back in time coincidence. The energy deposition in the liquid xenon detector, measured as the total sum

of the observed charge in all photomultipliers, should exceed a certain threshold. The trigger electronics comprises FADCs and FPGAs to realize this. Photomultiplier signals are digitized by the FADCs, and then, arithmetic calculations are performed in the FPGAs to decide whether to record or discard an event. In order to maintain the trigger quality during a long-term data acquisition, the results of detector calibration are reflected to the trigger system as needed.

Energy scale calibration is preformed primarily using CEX data. However, the CEX calibration is time consuming and the setup needs to be modified, which would cause loss of physics data acquisition time. Therefore, another method has been developed to monitor the energy scale around the signal region while simultaneously acquiring physics data. The data acquisition trigger system can generate 32 different types of trigger signals with proper prescaling. This enables us to mix the calibration data in the physics data to monitor the detector status at any given time. Among these types, there exists a trigger logic that is generated only using the deposited energy in the liquid xenon detector with a threshold of around 40 MeV. The events recorded using this trigger logic are dominated by muon radiative decays and positron annihilations in flight with a contamination of comic-ray events, as shown in Figure 13. The green and blue lines indicate contributions from radiative decay events and positron annihilations in flight, and cosmic-ray background events, respectively. The effect of detector resolution is taken into account in this description. It can be seen that the event distribution is well reproduced by the combined function shown in red. The end point of the green line can be precisely determined along with the acquisition of physics data, and this can be used to monitor the stability of the energy scale of the liquid xenon detector.

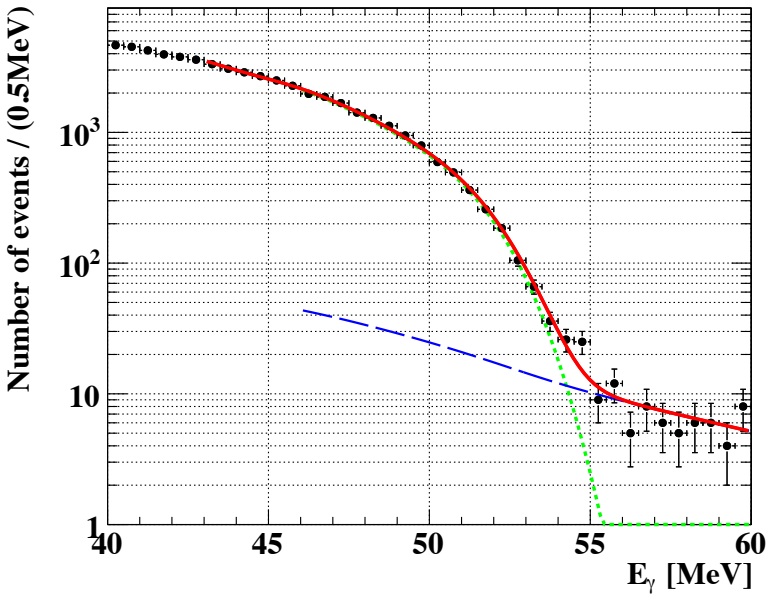

Figure 13. Energy distribution of observed photons around the end point of the radiative muon decay. The green and blue lines indicate contributions from radiative decay events and positron annihilations in flight, and cosmic-ray background events, respectively. The red line indicates the combined function of these two distributions.

3.4. Detector performance
Here, we summarize the best performance of the detector achieved so far. It should be noted that more precise calibration is in progress along with a better description of the detector by a simulation, which provides us with opportunities to improve the detector performance in the future.

3.4.1. Energy measurement The gamma-ray energy is reconstructed by summing up the number of photoelectrons observed by all photomultipliers. A small but significant correction is applied to achieve better resolution by taking the effect of the solid angle into account. The effect of non-uniform coverage of the photocathode is also corrected. Figure 14 shows a distribution of reconstructed gamma-ray energy in a CEX run for an energy deposition of 82.9 MeV on the NaI counter with an opening angle requirement between two photons larger than 175°. It is also required that the reconstructed position in the liquid xenon detector be located deeper than 2 cm from the inner face, so that events with energy leakage are removed from the active volume. The distribution is fitted with a combined function of a gaussian and an exponential

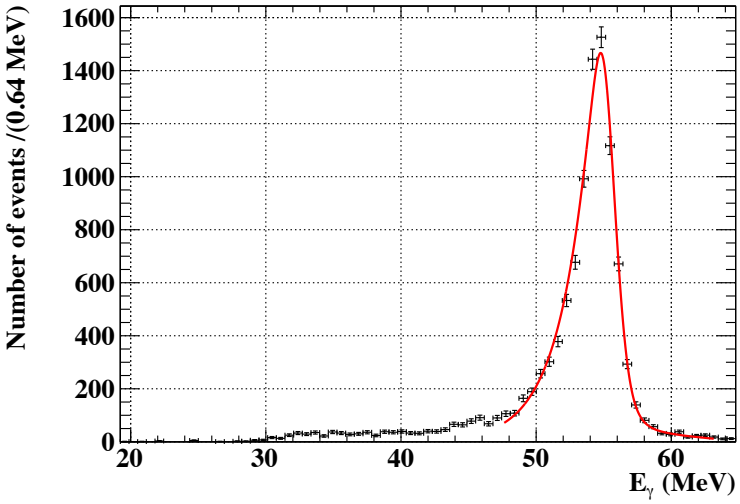

Figure 14. Measured energy spectrum of 54.9-MeV gamma rays.

function taking into account the pedestal distribution measured in the CEX run. An average energy resolution of $(5.8 \pm 0.35)\%$ in FWHM with a right tail of $\sigma_R = (2.0 \pm 0.15)\%$ is obtained.

3.4.2. Position reconstruction The gamma-ray interaction position in the active volume is reconstructed by comparing the light distribution observed by photomultipliers and solid angles covered by them viewed from the reconstructed position. The resolution of the position reconstruction is evaluated using lead collimators having thickness of 1.8 cm and 1-cm slits located in front of the liquid xenon detector. Figure 15 shows a distribution of the reconstructed position along the vertical direction with collimators in the CEX run. Three clear peaks corresponding to the shadow of the three slits are observed. A fitting for the distribution is overlaid in the figure. From these results, the resolution of the position reconstruction is estimated to be 5 mm by taking into account the effects of the slit width and the beam spread at the target.

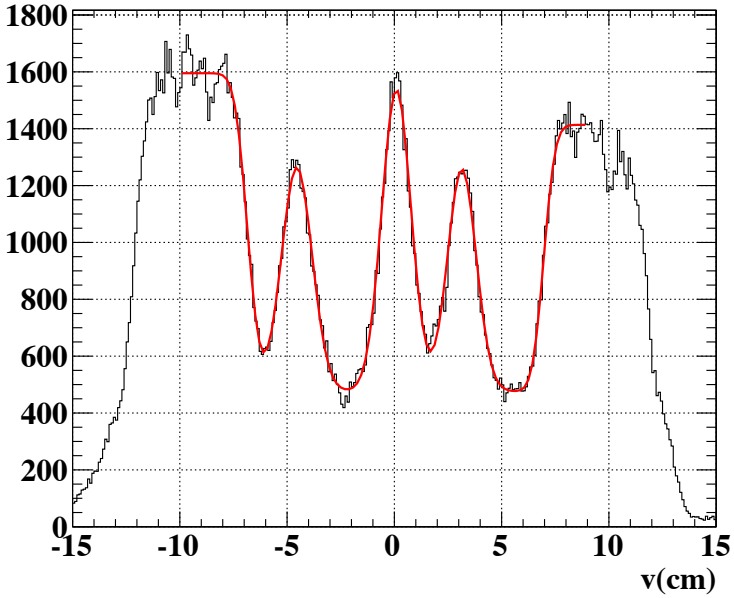

Figure 15. Distribution of reconstructed positions along vertical direction with collimators located in front of photon detector.

3.4.3. Time measurement The gamma-ray arrival time is calculated in the following manner. First, the scintillation photon arrival time at each photomultiplier is calculated by subtracting the propagation time of the scintillation photon in the liquid. Time offsets in signal transfer cables and electronics are subtracted during this calculation. Then, the gamma-ray interaction time is calculated by averaging the measured time at each photomultiplier with a weight of the number of photoelectrons. Figure 16 shows a distribution of the measured time difference between the liquid xenon detector and the plastic scintillation counters located in front of the NaI counter in the CEX run. A gamma-ray energy deposition of around 54.9 MeV is required at the xenon detector during the event selection. The distribution is fitted with a gaussian function, showing a spread of 135 ps in σ. The time resolution of the plastic scintillation counters is estimated to be 93 ps by carrying out an independent analysis. The beam spread of the π^- beam on the hydrogen target is estimated to be 58 ps equivalent in time. By subtracting these two contributions, we obtain a time measurement resolution of 78 ps in σ.

3.4.4. Detection efficiency The detection efficiency of the signal gamma ray is estimated to be 67% for photons with energies larger than 46 MeV by performing the Monte Carlo simulation, in which all the realistic information of materials used in the detector setup is incorporated. The efficiency is also calculated using the CEX run data for the 54.9-MeV gamma rays by requesting the 82.9-MeV gamma-ray observation in the NaI counter; an efficiency of 63% is obtained after subtracting the effect caused by a neutron background event from a radiative capture process ($\pi^- + \mathrm{p} \to \gamma + \mathrm{n}$) . The discrepancy of 4% between these two estimation is considered to be as an uncertainty. Thus, we conclude that the photon detection efficiency is $(63 \pm 4)\%$ in the range of $E_\gamma > 46$ MeV.

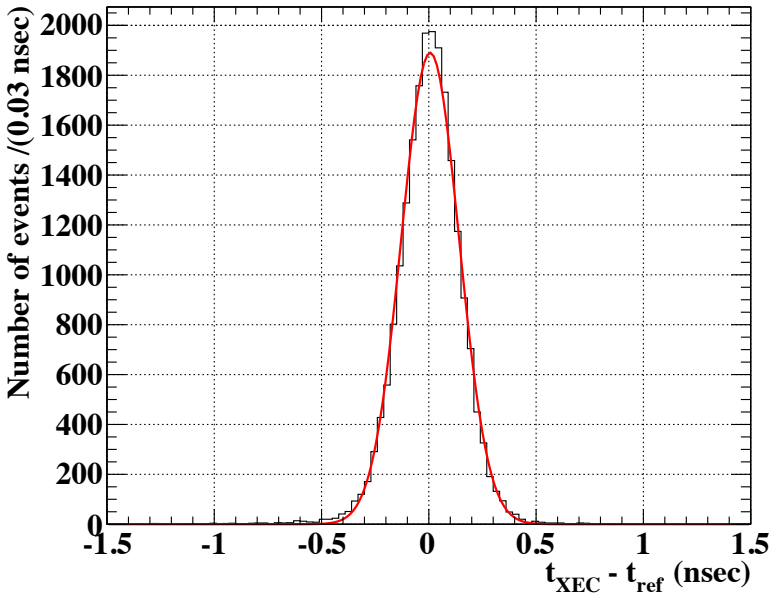

Figure 16. Measured time difference between photon detector and plastic scintillation counters located in front of NaI counter.

4. Summary

The MEG liquid xenon detector has been successfully constructed after extensive R&D activities for more than 10 years and is being operated without any major problems. This detector is the first instance of the application of a large-sized liquid xenon detector to a physics experiment. As expected, the detector shows outstanding features. We intend to further improve the detector performance by carrying out more precise calibration and gaining a better understanding of the detector based on simulation results.

References

[1] Aprile E *et al.* 2006 *Phys. Rev. Lett.* **97** 081302
[2] Yamashita M *et al.* Astro. Phys. **20** 79
[3] MEGA Collaboration Ahmed M *et al.* 2002 *Phys. Rev.* D **65** 112002
[4] Mori T *et al.* 1999 *Research Proposal to PSI* R99-05
[5] Nishiguchi H 2007 *Nucl. Phys.* B **172** 266
[6] Cattaneo P W 2010 *Nucl. Instru. and Meth.* A in press
[7] Ootani W *et al.* 2005 *IEEE Trans. Applied Superconductivity* **14** 568
[8] MEG Collaboration Adam J *et al.* 2010 *Nucl. Phys.* B **834** 1
[9] Ritt S *et al.* 2002 *Nucl. Instr. and Meth.* A **494** 520
[10] Mihara S *et al.* 2002 *IEEE Trans. Nucl. Sci.* **49** 588
[11] Mihara S *et al.* 2004 *Nucl. Instr. and Meth.* A **518** 45
[12] Haruyama T *et al.* 2004 *AIP Conf. Proc.* **710** 1459
[13] Baldini A *et al.* 2005 *Nucl. Instr. and Meth.* A **545** 753
[14] Iwamoto T *et al.* 2008 *Cryogenics* **49** 254
[15] Baldini A *et al.* 2006 *Nucl. Instr. and Meth.* A **565** 589
[16] Mihara S *et al.* 2004 *Cryogenics* **44** 223
[17] Mihara S *et al.* 2006 *Cryogenics* **46** 688
[18] Doke T 1981 *Portugal Phys.* **12** 9